Cell Death & Differentiation (2020) 27:676–694
https://doi.org/10.1038/s41418-019-0379-5

Cell Death & Differentiation

ARTICLE

RUNX3 suppresses metastasis and stemness by inhibiting Hedgehog signaling in colorectal cancer

Bo Ram Kim[1] · Yoo Jin Na[2] · Jung Lim Kim[1] · Yoon A. Jeong[2] · Seong Hye Park[2] · Min Jee Jo[2] · Soyeon Jeong[1] · Sanghee Kang[3] · Sang Cheul Oh[1] · Dae-Hee Lee[1]

Received: 30 October 2018 / Revised: 29 May 2019 / Accepted: 18 June 2019 / Published online: 5 July 2019

Abstract

Disabled tumor suppressor genes and hyperactive oncogenes greatly contribute to cell fates during cancer development because of their genetic alterations such as somatic mutations. However, little is known about how tumor suppressor genes react to diverse oncogenes during tumor progression. Our previous study showed that RUNX3 inhibits invasiveness by preventing vascular endothelial growth factor secretion and suppressed endothelial cell growth and tube formation in colorectal cancer (CRC). Hedgehog signaling is crucial for the physiological maintenance and self-renewal of stem cells, and its deregulation is responsible for their tumor development. The mechanisms that inhibit this pathway during proliferation remain poorly understood. Here, we found that the tumor suppressor RUNX3 modulates tumorigenesis in response to cancer cells induced by inhibiting oncogene GLI1 ubiquitination. Moreover, we demonstrated that RUNX3 and GLI1 expression were inversely correlated in CRC cells and tissues. We observed a direct interaction between RUNX3 and GLI1, promoting ubiquitination of GLI1 at the intracellular level. Increased ubiquitination of GLI1 was induced by the E3 ligase β-TrCP. This novel RUNX3-dependent regulatory loop may limit the extent and duration of Hedgehog signaling during extension of the tumor initiation capacity. On the basis of our results, identification of agents that induce RUNX3 may be useful for developing new and effective therapies for CRC.

Introduction

The development of tumor cells often results from multiple genetic alterations that cause a cellular shift. Numerous specific genetic alterations have been identified that activate proto-oncogenes or inactivate tumor suppressor genes. Indeed, the sine qua non of a tumor gene is that it is affected by a mutational event with a vital prevalence. In addition, a 'third' pathway to tumorigenesis has been identified whereby the expression of key genes is regulated through promoter hypermethylation and silencing. Particularly, tumor suppressor genes may be subject to this mechanism of inactivation, in addition to mutational events. Oncogenes and tumor suppressor genes have classically been assigned distinct, independent roles in tumor progression. However, the relationships between these tumor-promoting processes remain poorly understood.

The human RUNX gene is homologous to the Drosophila genes *Runt* and *Lozenge* [1, 2] and encodes a subunit of the Runt-domain transcription factor PEBP2/CBF [3]. The Runt-related transcription factor (RUNX) family includes RUNX1, RUNX2, and RUNX3, which play a role in cell proliferation and differentiation in humans [4, 5]. RUNX3 has been shown to act as a tumor suppressor in gastric cancer [6], and previous studies have indicated that it is downregulated in various tumors [7]. Moreover, inactivation of RUNX3 is caused by promoter hypermethylation, loss of heterozygosity, or

Edited by G. Del Sal

Supplementary information The online version of this article (https://doi.org/10.1038/s41418-019-0379-5) contains supplementary material, which is available to authorized users.

✉ Sang Cheul Oh
sachoh@korea.ac.kr

✉ Dae-Hee Lee
neogene@korea.ac.kr

[1] Department of Oncology, Korea University Guro Hospital, Korea University College of Medicine, Seoul, Republic of Korea

[2] Graduate School of Medicine, Korea University College of Medicine, Seoul, Republic of Korea

[3] Department of Surgery, Korea University Guro Hospital, Korea University College of Medicine, Seoul, Republic of Korea

mislocalization [8, 9]. Various studies have demonstrated that RUNX3 can function as a tumor suppressor by regulating metastasis in cancer [10, 11]. However, the inhibition mechanism of metastasis mediated by RUNX3 remains unclear. Along with this, whether RUNX3 and stemness are correlated is unknown. Cancer stem cells (CSCs) play critical roles in tumor growth, metastasis, recurrence, and drug resistance [12, 13]. Various signaling pathways have been involved in CSCs, such as the Hedgehog (Hh), Wnt, and Notch signaling pathways [14–16]. CSCs have been considered to have a function in the generation of niches for metastasis. Therefore, targeting of metastasis and CSCs is an important strategy for cancer therapy.

The Hh signaling pathway is essential in tissue polarity, patterning maintenance, and stem cell renewal during embryonic development. The Hh signaling pathway in mammals, there are three homolog ligands, Sonic Hedgehog (SHh), Indian Hegehog (IHh), and Desert Hedgehog (DHh). All Hedgehog ligands binds with the Patched (PTCH1) transmembrane receptors, results in activates the smoothened transmembrane receptor and glioma-associated oncogene (GLI) transcriptional activators [17]. We and other researchers have demonstrated that the Hh pathway plays an important role in cancer proliferation, metastasis, angiogenesis, and stemness [18–20]. Hh signaling activates the GLI family of zinc-finger transcription factors to regulate their target genes. Three GLI proteins, GLI1, GLI2, and GLI3, have been identified in mammals [21]. GLI2 and GLI3 contain both C-terminal transcriptional activation and N-terminal repression domains. However, GLI1 has only a C-terminal transcriptional activation domain and thus is the major transcriptional activator of Hh target genes [22]. Thus, GLI1 is considered a key factor in the Hh signaling pathway [23]. The stability of GLI1 is regulated by three E3 ubiquitin ligases: the Skp/Cul/F-box complex $SCF^{\beta\text{-}TrCP}$, E3 ligase ITCH in conjunction with the adaptor NUMB, and E3 ligase p300/CREB-binding protein-associated factor (PCAF) [24, 25]. RUNXs were reported to be linked to major developmental pathways, such as the transforming growth factor-β, Wnt, and Hh signaling pathways [26]. RUNX2 has also been associated with IHh [27]. In this study, we found for the first time that RUNX3 negatively regulated GLI1 expression. In addition, RUNX3 interacted directly with GLI1. Clinically, loss of RUNX3 and increased GLI1 predicted poor survival and metastasis in patients with human colorectal cancer (CRC). Overexpression of RUNX3 enhanced the ubiquitination of GLI1. Our data suggest that overexpression of RUNX3 prevents metastasis and reduces cancer stem-like cell populations through GLI1 degradation. Both oncogenes and tumor suppressor genes have been implicated in carcinogenesis and cancer progression, and have been long regarded as independent; however, we hypothesized that these distinct genetic elements are related through epigenetic mechanisms. Our model suggests that *RUNX3* silences the *GLI1* oncogene through protein degradation induced by ubiquitination in CRC cells.

Materials and methods

Patients and tissue specimens

A total of 197 cases of colon cancers were collected from the Korea University Guro Hospital tissue bank between 2000 and 2006. The patients with colon carcinoma include 109 male and 88 female. This protocol was reviewed and approved by the Institutional Review Board of Guro Hospital (KUGH 12110).

Plasmid construction

To prepare the RUNX3 overexpression vector, we cloned RUNX3 between the HindIII and BamHI restriction sites of the pFlag-c1 vector. Vectors of pCS4-3myc-RUNX3 (full-length) and RUNX3 deletion mutant vectors fused with the Myc tag were kindly provided by Dr. SC Bae at Chungbuk National University.

Cell culture and stable cell lines

Human CRC cells were purchased from the Korea Cell Line Bank. Cells were cultured in RPMI 1640 medium (Invitrogen, Carlsbad, CA, USA) containing 10% fetal bovine serum (HyClone, Logan, UT, USA), 1 mM L-glutamine, and 26 mM sodium bicarbonate for monolayer cell culture. Tumor sphere media (also referred to as serum-free medium, SFM) was composed of DMEM/F12 media supplemented with 1x B27 (Invitrogen), EGF (20 ng/mL, Peprotech, Rocky Hill, NJ, USA), bFGF (10 ng/mL, Peprotech), 200 U/mL penicillin, and 200 μg/mL streptomycin. For stable RUNX3 overexpression, we transfected the cells with pFlag-c1 or pFlag-c1 RUNX3, using Lipofectamine 2000 (Invitrogen) and selected transfectants using puromycin. For stable knockdown, we used RUNX3 shRNA or GLI1 shRNA from Santa Cruz Biotechnology (Dallas, TX, USA). SNU283 cells were treated with 5 μg/mL Polybrene (Santa Cruz Biotechnology). The cells were infected by adding the RUNX3 shRNA or GLI1 shRNA lentiviral particles. The next day, SNU283 cells were cultured in medium containing puromycin. Stable infected cells were selected using puromycin.

Reagents and antibodies

GANT 61 was purchased from Selleckchem (Houston, TX, USA). 5-Aza-2′-deoxycytidine and cyclohexamide were purchased from Sigma (St. Louis, MO, USA). Protein G PLUS-Agarose, anti-Snail, anti-EpCAM, anti-Myc, anti-PCAF,

anti-LaminB, anti-SHH, and anti-Ub were from Santa Cruz Biotechnology; anti-GLI1, anti-Sox2, anti-Oct4, anti-β-TrCP, and Anti-SUFU were from Cell Signaling Technology (Danvers, MA, USA); anti-N-cadherin, ITCH, and E-cadherin were from BD Biosciences (Franklin Lakes, NJ, USA). anti-RUNX3, anti-LGR5, anti-GLI2, anti-GLI3, and anti-Nanog were from Abcam (Cambridge, UK); anti-CD133 was from Miltenyi Biotec (Bergisch Gladbach, Germany); anti-actin antibody was from Sigma. The secondary antibodies, anti-mouse IgG horseradish peroxidase and anti-rabbit IgG horseradish peroxidase were from Cell Signaling Technology.

Immunoblotting

Cells were lysed in RIPA buffer (50 mM Tris, 150 mM NaCl, 1% Triton X-100, 0.1% SDS, and 1% sodium deoxycholate [pH 7.4]) with protease inhibitor and phosphatase inhibitor cocktails and subjected to SDS-PAGE. Cells were then transferred onto nitrocellulose membranes (GE Healthcare Life Sciences, Little Chalfont, UK), blocked with Tris-buffered saline containing 0.2% Tween 20 and 5% skim milk, incubated with primary antibody, and then incubated with horseradish peroxidase-labeled secondary antibody. The signals were detected using X-ray film.

Wound healing assay and Matrigel invasion assay

After transfection, cells were seeded at 5×10^5 cells/well in 12-well plates. At 100% confluence, two parallel wounds were made using a plastic pipette tip. Cells were then grown in culture medium containing 5% fetal bovine serum. Images of the wound were collected at 0, 24, and 48 h using a microscope. The migration rate was quantified by measuring the distance between the wound edges. This assay was independently repeated three times. For the Matrigel invasion assay, 3×10^5 cells/well were seeded in the upper chamber, which was coated with Matrigel (BD Biosciences). After 48 h at 37 °C and 5% CO_2, the cells present on the lower surface of the insert were stained with Diff-Quik stain (Biochemical Sciences, Inc., Swedesboro, NJ, USA). The cells that invaded through the Matrigel-coated membrane were counted by microscopy.

Immunofluorescence staining

Cells grown on glass coverslips were fixed with 3.7% formaldehyde for 15 min, followed by permeabilization with 0.5% Triton X-100 for 15 min at room temperature. Cells were then blocked 1 h with 3% bovine serum albumin. Primary antibodies were applied overnight at 4 °C, followed by incubation with Alexa Fluor 594-conjugated secondary antibody (Molecular Probes, Eugene, OR, USA) or fluorescein isothiocyanate (FITC)-conjugated secondary antibody (Sigma-Aldrich). The nuclei were costained with 4,6-diamidino-2-phenylindole (DAPI) and visualized by fluorescence microscopy.

Real-time PCR (RT-PCR)

Total RNA was extracted with Trizol reagent (Life Technologies, Carlsbad, CA, USA). Transcripts were amplified using a reverse transcriptase polymerase chain reaction kit (Life Technologies). Real-time PCR was performed on an Applied Biosystems 9700 real time PCR machine using gene specific oligonucleotide primers for Taqman probes (Applied Biosystems, Foster City, CA. USA). Taqman probes were as follows: GAPDH (Hs99999905_m1), Nanog (Hs04260366_g1), Oct4 (Hs00153294_m1), Sox2 (Hs01053049_s1), LGR5 (Hs00173664_m1), GLI1 (Hs01110766_m1), RUNX3 (Hs00231709_m1), PTCH1 (Hs00216017_m1), VEGFC (Hs01099203_m1), VEGFD (Hs01128657_m1), SNAIL (Hs00195591_m1), and cyclin D1(Hs00765553_m1). Gene expression was normalized to the GAPDH mRNA levels.

Luciferase assay

Cells were plated at a density of 5×10^4 cells per well in 6-well plates and transfected with the $8 \times 3'$Gli-BS or pGL4-phGLI1 (RIKEN, Tokyo, Japan) and internal control Renilla luciferase construct. Cell were lysed in 100 μL lysis buffer (Promega, Madison, WI, USA) for 15 min at room temperature. Lysed samples were transferred into 96-well plates, and 50 μL firefly substrate (Promega) was added to the samples. After measuring firefly luciferase activity, 50 μL Stop & Glo® buffer (Promega) added to the cell lysates. Dual-luciferase activity was measured using a Glomax luminometer following the manufacturer's instructions.

Apoptosis and cell cycle analyses

HT29 and SNU283 cells were mixed with 1.25 μL Annexin V and 7 μL performing propidium iodide (PI) reagent (BioBud, Seoul, Korea, Cat. LS-02-100) and incubated for 10 min at 4 °C in the dark. Staining was terminated, and the cells were immediately analyzed by flow cytometry. HT29 and SNU283 cells were harvested by trypsin and then were fixed with 5 mM EDTA and 85% ethanol. Fixed cells were incubated with 50 μg/mL PI and 20 μg/ml RNase at 37 °C for 30 min and were analyzed by performing flow cytometry.

Self-renewal assay

HT29 and SNU283 cells (1 cell/μL in SFM) were seeded at 100 μL/well in 96-well plates for 7 days. The total number of spheres in each well was counted under a microscope.

Next, the cells were dissociated and stained with Trypan blue (Amresco Inc., Solon, OH, USA).

Detection of CD133 and EpCAM by FACS analysis

The cells were washed with cold PBS, and subsequent cell suspensions were incubated at 4 °C with 1:10 FITC-conjugated monoclonal CD133 antibody (Miltenyi Biotec) and PE-conjugated monoclonal EpCAM antibody (Miltenyi Biotec) for 1 h in the dark. After incubation, the cell pellets were resuspended in a suitable amount of buffer for analysis by flow cytometry.

Co-Immunoprecipitation (Co-IP)

Cells were washed with ice-cold PBS and incubated on ice for 5 min with 300 μL lysis buffer (Cell Signaling Technolog, Cat. No. 9803) (1 mM PMSF, protease inhibitor, and phosphatase inhibitor). The cells were scrape-harvested, cellular debris was removed by centrifugation for 5 min at 15,000 rpm at 4 °C, and the concentration of protein was determined by BCA assay (Thermo Fisher Scientific, Waltham, MA, USA). Cell supernatants were incubated with primary antibody overnight at 4 °C, followed by addition of 50 μL protein G agarose beads (50% slurry) for 2 h at 4 °C. Immunoprecipitates were washed five times with cold lysis buffer, separated by centrifugation for 30 s at 10,000 rpm, and then heated with 2× sample buffer for electrophoresis and western blot analysis.

Immunohistochemical staining and assessment

Section of formalin-fixed, paraffin-embedded tumor specimens were deparaffinized in xylene and rehydrated in graded alcohol. Endogenous peroxidase was blocked using 3% hydrogen peroxide in dH_2O for 15 min. Antigen retrieval was performed with cooker for 20 min. The specimens were incubated in universal blocking solution for 15 min at room temperature, and then incubated at 4 °C overnight with primary antibodies. Antibodies, clones, and dilutions used in this method are listed in Table 1. The samples were incubated with peroxidase-conjugated anti-goat IgG for 1 h at room temperature. IHC reactions were visualized by diaminobenzidine staining, using a DAKO EnVision + system (Agilent Technologies, Santa Clara, CA, USA) (Table 2).

Small interfering RNA transfection

Small interfering RNA (siRNA) duplexes specific to GLI1 and β-TrCP were synthesized by Invitrogen and Dharmacon (Lafayette, CO, USA). SUFU siRNA were from Santa Cruz Biotechnology. As a non-specific control siRNA, a scrambled siRNA duplex was used. Transfection was performed using RNAiMAX reagent (Invitrogen) following the manufacturer's instructions

Table 1 Antibodies used for immunohistochemical staining

Antibody	Source	Clone number	Dilution
RUNX3	Abcam[a]	R3-5G4	1:100
GLI1	Santa Cruz Biotechnology[b]	N-16	1:100

[a]Cambridge, UK

[b]Dallas, TX, USA

Table 2 IHC scoring

Percentage score (PS)	Observation	Intensity score (IS)	Observation
1	0–5%	0	None
2	6–25%	1	White brown
3	26–50%	2	Brown
4	51–75%	3	Dark brown
5	76–100%		

GST pull-down assay

The cDNA of GLI1 was inserted into pGEX-4T-1. The protein was overexpressed in *Escherichia coli* induced 1 mM IPTG overnight at 16 °C. Glutathione agarose resin (Pierce™ GST Protein Interaction Pull-Down Kit; Thermo Fisher Scientific) balanced with equilibrium buffer was utilized to capture the proteins into complexes according to the manufacturer's instructions. Thereafter, the complexes were incubated with lysate of HT29 pFlag-c1 or pFlag-c1 RUNX3, elution buffer was used to separate the combined proteins and the eluted proteins were analyzed by western blotting.

Chromatin immunoprecipitation (ChIP) assay

For ChIP, 1.5×10^6 HT29 cells were cross-linked with 1% formaldehyde at 37 °C for 10 min. After washing and spinning, the cell pellets were lysed with SDS lysis buffer (PMSF and protease inhibitor) on ice for 10 min. The cell lysate was sonicated to shear the DNA to obtain fragments between 200 and 1000 base pairs. The lysates were immunoprecipitated with anti-RUNX3 overnight at 4 °C. The protein-DNA complex was collected with protein A salmon sperm DNA, eluted, and reverse cross-linked. Following treatment with protease K, EDTA, and Tris-HCl, DNA fragments were extracted with phenol/chloroform and precipitated with ethanol. The DNA was analyzed by PCR using the following specific primers: RUNX3BS1 forward, 5′-CTA CAG CTC CCT GCT CAC TTT T-3′; reverse, 5′-CCA CTA GAG GGC AGA GTT AAG GTA-3′; RUNX3BS2 forward, 5′-CTC CAG AAC TTC GAG ACG TAG AG-3′; reverse, 5′-CTG GAA GAA GGT GAG

GAG TCT A-3′; RUNX3BS3 forward, 5′-CCA TAG ACT CCT CAC CTT CTT C-3′; reverse, 5′-AAT AGT GGA GGT AGG GTA GTC G-3′.

Gene expression analysis

To investigate the correlation with human mRNA expression, The Cancer Genome Atlas (TCGA) dataset was used. The TCGA dataset was downloaded from Xena Browser (https://xena.ucsc.edu) on 15 August 2018 and used IlluminaHiSeq ($n = 329$) in TCGA Colon Cancer (COAD) of TCGA hub. This dataset was processed with RSEM normalized count and $\log2(x + 1)$ by downloading level 3 RNA sequencing data from the TCGA data coordination center. In the dataset, the primary tumor samples were selected, and the correlation between mRNAs was estimated by the Pearson correlation coefficient. Statistical analyses were conducted using R version 3.5.0 (R Foundation for Statistical Computing, Vienna, Austria). A p value <0.05 was considered as significant.

In vivo metastasis model

The metastasis model was established to determine the effect of RUNX3 on tumor metastasis. HT29 and SNU283 cells (1×10^6) were intravenously injected into the tail veins of BALB/c nude mice. After 9 weeks, the mice ($n = 7$) were sacrificed and lung tissues were analyzed to detect the occurrence of metastasis. The sections were stained with hematoxylin and eosin (H&E) and analyzed for the presence of metastasis.

Statistical analysis

Statistical analysis was performed with GraphPad InStat 6 software (GraphPad Software, Inc., La Jolla, CA, USA). The Student's t-test was used to analyze the data of experiments involving two groups. Pearson correlation coefficient was used to analyze the correlation between RUNX3 and GLI1. Significances between two groups were evaluated by the Mann Whitney test. Kaplan–Meier survival curves was used to determine survival analysis, and the differences in survival curves were evaluated using the log-rank test. A p-value of <0.05 was considered as significant.

Results

Inverse correlation between RUNX3 and GLI1 in CRC cell lines

To study the relationship between RUNX3 and GLI1 in CRC, we first confirmed the expression of both proteins in CRC cell lines. Compared with CRC cells with low RUNX3 expression, RUNX3 overexpressing cells had relatively low GLI1 expression in CRC cell lines (Fig. 1a). Consistent with the results at the protein level, the mRNA expression levels also indicated an inverse correlation between RUNX3 and GLI1 in CRC cell lines (Fig. 1b). We also examined RUNX3 and GLI1 expression in fresh-frozen CRC tissues. RUNX3 was overexpressed in normal colon tissues compared with that in CRC tissues. Whereas, GLI1 was overexpressed in CRC tissue compared with that in normal colon tissues (Fig. 1c). Overexpression of RUNX3 inhibited GLI1 expression at both the protein and mRNA levels, whereas knockdown of RUNX3 enhanced GLI1 expression (Fig. 1d, e). In agreement with these observations, immunofluorescence studies also confirmed that overexpression of RUNX3 inhibited GLI1 expression, while knockdown of RUNX3 enhanced GLI1 expression (Fig. 1f). These results were also confirmed by fractionation of the nuclei and cytosol (Supplementary Fig. 1A). To examine the effect of RUNX3 silencing on GLI1 function, we co-transfected the $8 \times 3'$Gli-BS-luciferase reporter into HT29 and SNU283 cells. Overexpression of RUNX3 significantly reduced GLI transcriptional activity, whereas knockdown of RUNX3 enhanced GLI transcriptional activity (Fig. 1g). To examine whether GLI1 regulates RUNX3, we determined the effect on RUNX3 expression by altering GLI1 expression. Overexpression and knockdown of GLI1 expression did not affect RUNX3 expression (Supplementary Fig. 1B). Next, we examined whether RUNX3 regulates GLI1 target genes. Overexpression of RUNX3 decreased the mRNA levels of GLI1 target genes, whereas knockdown of RUNX3 increased the mRNA levels of GLI1 target genes (Fig. 1h and Supplementary Fig. 1C). As well known, RUNX3 is inactivated by promoter hypermethylation [9]. HT29 cells in which the RUNX3 promoter is hypermethylated were treated with 5-Aza-dc (5-aza-2′-deoxycytidine, DNA methylated inhibitor). 5-Aza increased the expression of RUNX3 in HT29 cells. Increased RUNX3 inhibited the expression of GLI1 (Fig. 1i). These results indicate that RUNX3 negatively regulates GLI1 expression.

Inverse correlation between RUNX3 and GLI1 in clinical CRC specimens

Next, we examined whether RUNX3 is associated with GLI1 in human CRC tissues. Immunohistochemistry (IHC) analysis was performed to confirm RUNX3 and GLI1 expression. As shown in Fig. 2a, staining of RUNX3 was observed in the nuclear compartment, while that of GLI1 was observed in both cytoplasm and nuclear compartments. RUNX3 was highly expressed in normal colon tissue. But was lost in tumors. In contrast, GLI1 was rarely expressed in normal colon tissue but highly expressed in tumors ($p < 0.0001$). As shown in Supplementary Fig. 2A, RUNX3 expression was generally higher in stages I and II than in

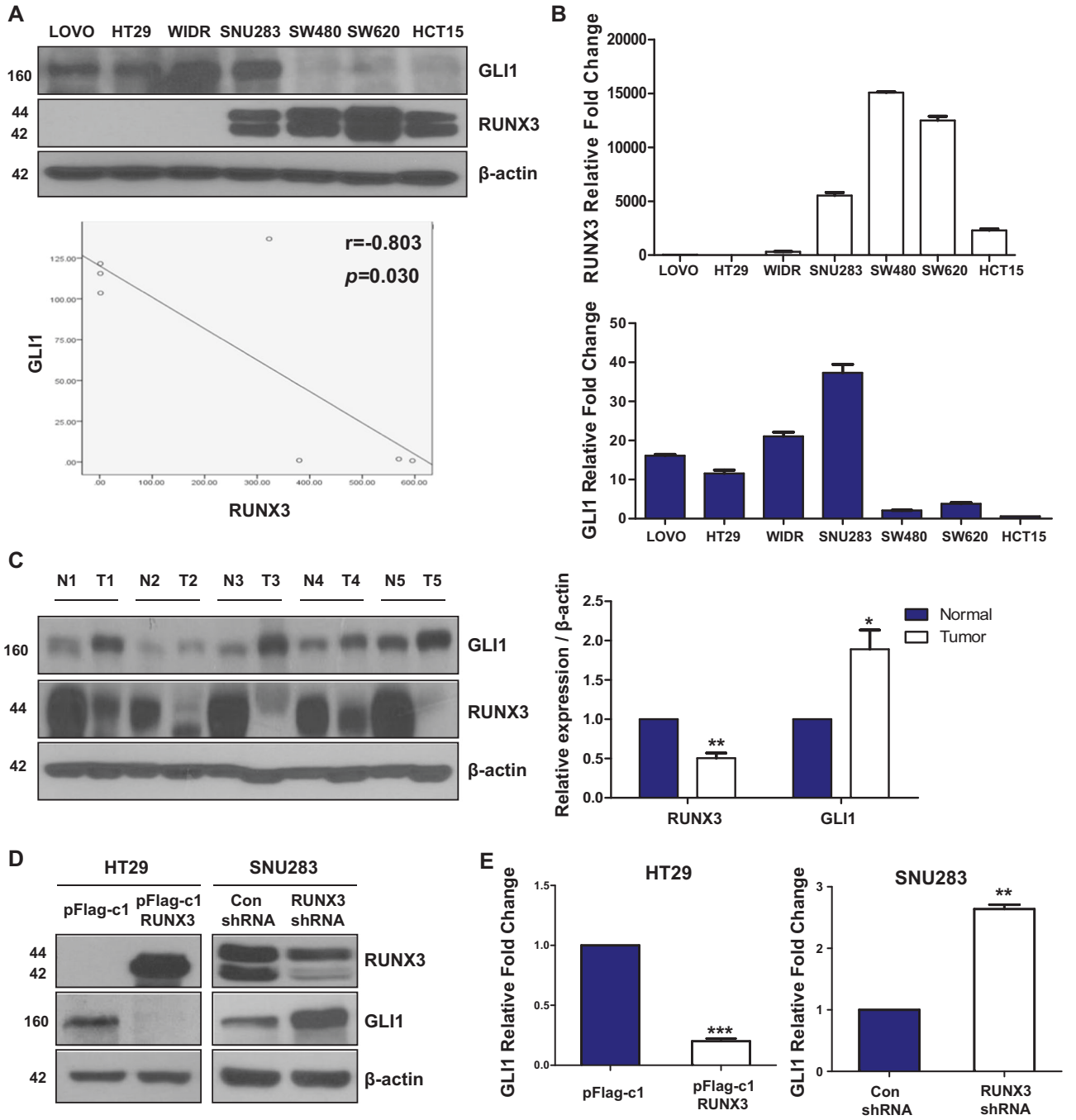

Fig. 1 Inverse correlation between RUNX3 and GLI1 in CRC cell lines. **a** RUNX3 and GLI1 protein levels in CRC cell lines were determined by western blotting. β-actin was used as a loading control ($p = 0.030$, Pearson's r). **b** RUNX3 and GLI1 mRNA levels in CRC cell lines were measured using real-time PCR. The expression was normalized to that of GAPDH. **c** RUNX3 and GLI1 expression in fresh-frozen CRC tissues was confirmed using western blot analysis. β-actin was used as a loading control. Quantitative graphs of signal intensity of RUNX3 and GLI1 are shown in the right panel and were prepared using ImageJ (NIH, Bethesda, MD, USA). N: Normal, T: Tumor. **d** Expression of GLI1 protein in RUNX3 overexpressing cells or RUNX3 knockdown cells was measured by western blot. β-actin was used as a loading control. **e** The expression of GLI1 mRNA in RUNX3 overexpressing cells or RUNX3 knockdown cells was measured by real-time PCR. The expression was normalized to that of GAPDH. **f** Immunofluorescence of RUNX3 and GLI1 was detected by confocal laser-scanning microscopy (original magnification, ×40). Scale bar, 10 μM. **g** GLI-luciferase activity by expression of RUNX3. Cells were transfected with a GLI-dependent luciferase reporter construct. The luciferase activity was normalized to that of pRL-TK vector. The controls (pFLAG-c1, Con shRNA) were equated to 1. **h** Expression of *GLI1*, *PTCH1*, *VEGFC*, *VEGFD*, *CyclinD1*, and *Snail* in RUNX3 overexpressing cells or RUNX3 knockdown cells was measured by real-time PCR. The expression was normalized to that of GAPDH. **i** HT29 cells were pretreated with 20 μM of 5-Aza-dc for 4 days and then treated with 20 ng/mL. The expression of GLI1 and RUNX3 was measured by western blotting. β-actin was used as a loading control. The data are expressed as the means of three independent experiments (*$p < 0.05$, **$p < 0.01$, ***$p < 0.001$, Student's t-test)

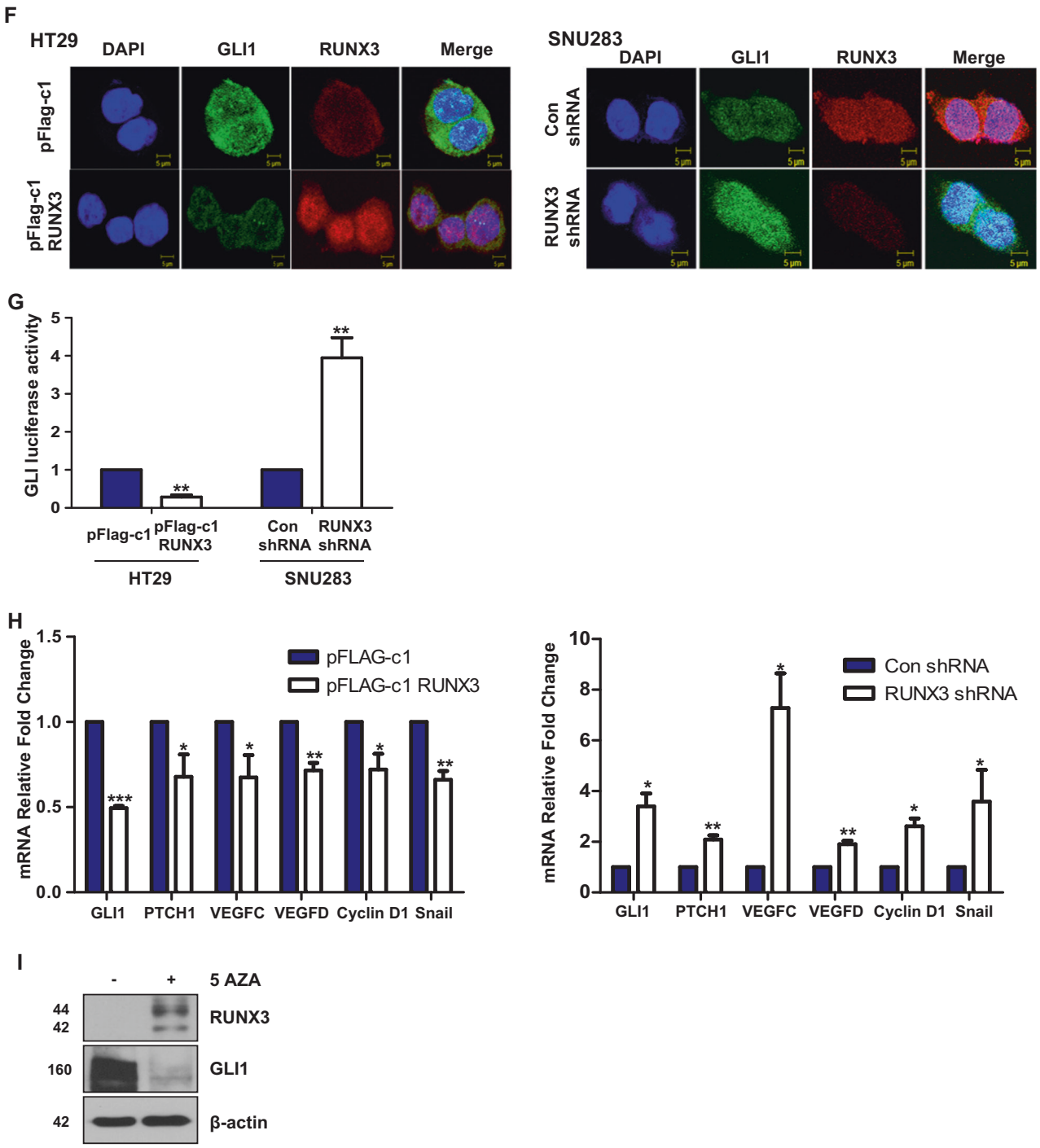

Fig. 1 (Continued)

stages III and IV ($p = 0.0034$). GLI1 expression was higher in stages III and IV than in stages I and II. The expression of RUNX3 was significantly higher in colon tissues with non-metastasis than in tissues with metastasis ($p = 0.037$). In contrast, the expression of GLI1 was significantly higher in colon tissues with metastasis than in tissues without metastasis ($p = 0.026$) (Fig. 2c). Furthermore, the expression of RUNX3 was higher in colon tissues with non-lymph node metastasis than that in tissues with lymph node metastasis ($p = 0.015$). The expression of GLI1 was higher in colon tissues with lymph node metastasis than that in tissues without lymph node metastasis ($p = 0.089$) (Fig. 2d). The contradictory effects of RUNX3 and GLI1 on survival were shown by the survival analysis. RUNX3-High patients showed better survival rates than RUNX3-Low patients ($p < 0.0001$), whereas GLI1-High patients showed

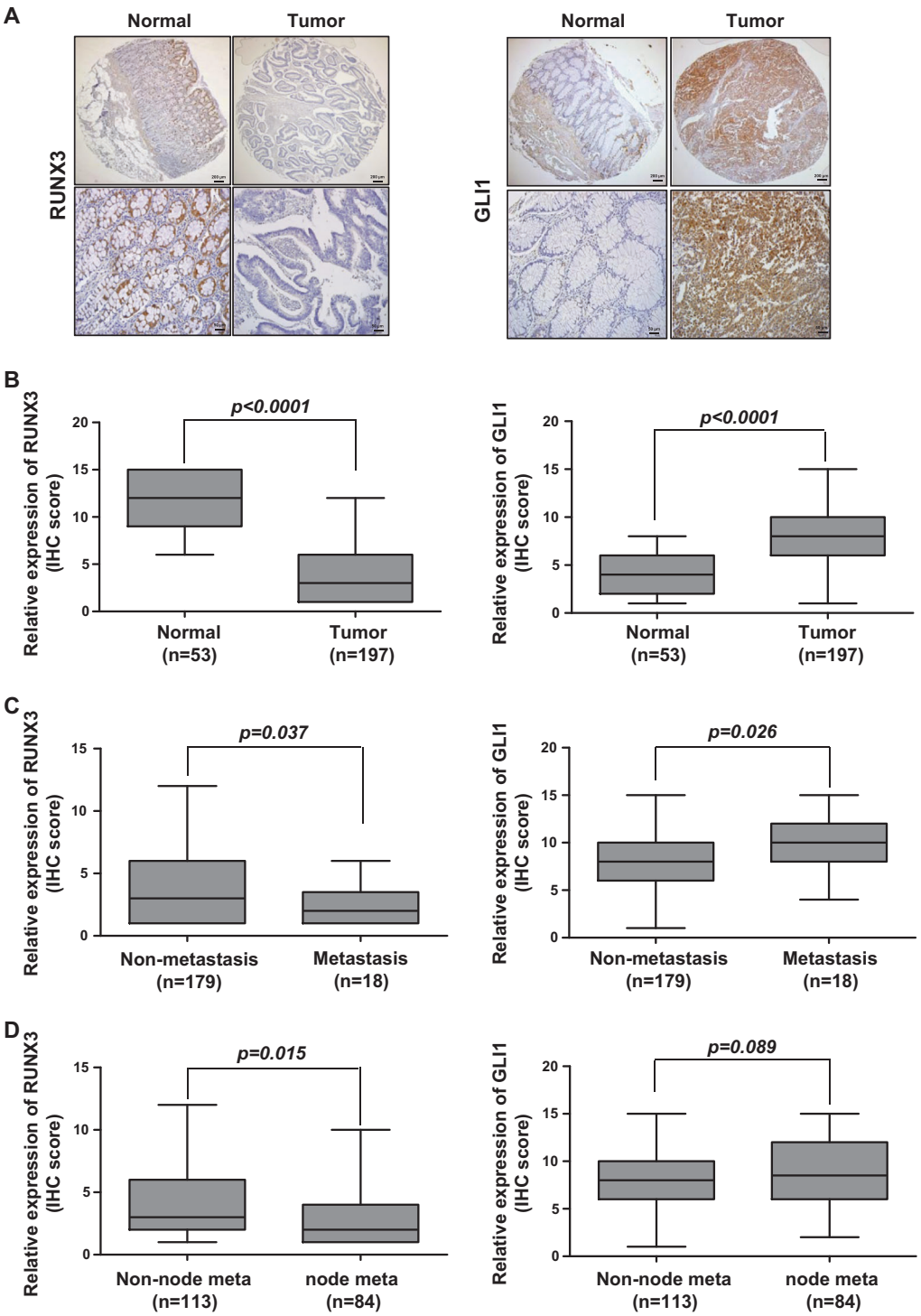

Fig. 2 Inverse correlation between RUNX3 and GLI1 in clinical CRC specimens. **a** Representative picture of IHC on human CRC specimens stained for RUNX3 and GLI1. Magnification ×4 (upper) and ×20 (lower). **b** Box plots indicate the percentage of RUNX3 positive tissues in normal and tumor samples (left). Box plots indicate the percentage of GLI1 positive tissues in normal and tumor samples (right). For normal versus tumor tissues: normal, $n = 53$, tumor, $n = 197$ ($p < 0.0001$, Mann Whitney). **c** Box plot representing the RUNX3 and GLI1 staining score in CRC tissues with and without metastasis. No metastasis, $n = 179$, Metastasis, $n = 18$ ($p = 0.037$, $p = 0.026$, Mann Whitney). **d** Box plot representing the RUNX3 and GLI1 staining score in CRC tissues with and without node metastasis. No node metastasis, $n = 113$, node Metastasis, $n = 84$ ($p = 0.015$, $p = 0.089$, Mann Whitney). **e**, **f** Overall survival of the colon cancer patients with RUNX3 and GLI1 expression was calculated and presented by Kaplan–Meier analysis, and RUNX3 and GLI1 expression correlated significantly with overall survival ($p < 0.0001$, $p = 0.0005$, Kaplan–Meier). **g**, **h** Overall survival of the Stage I and II colon cancer patients with RUNX3 and GLI1 expression was calculated and presented by Kaplan–Meier analysis, and RUNX3 and GLI1 expression correlated significantly with overall survival ($p < 0.0001$, $p = 0.037$, Kaplan–Meier)

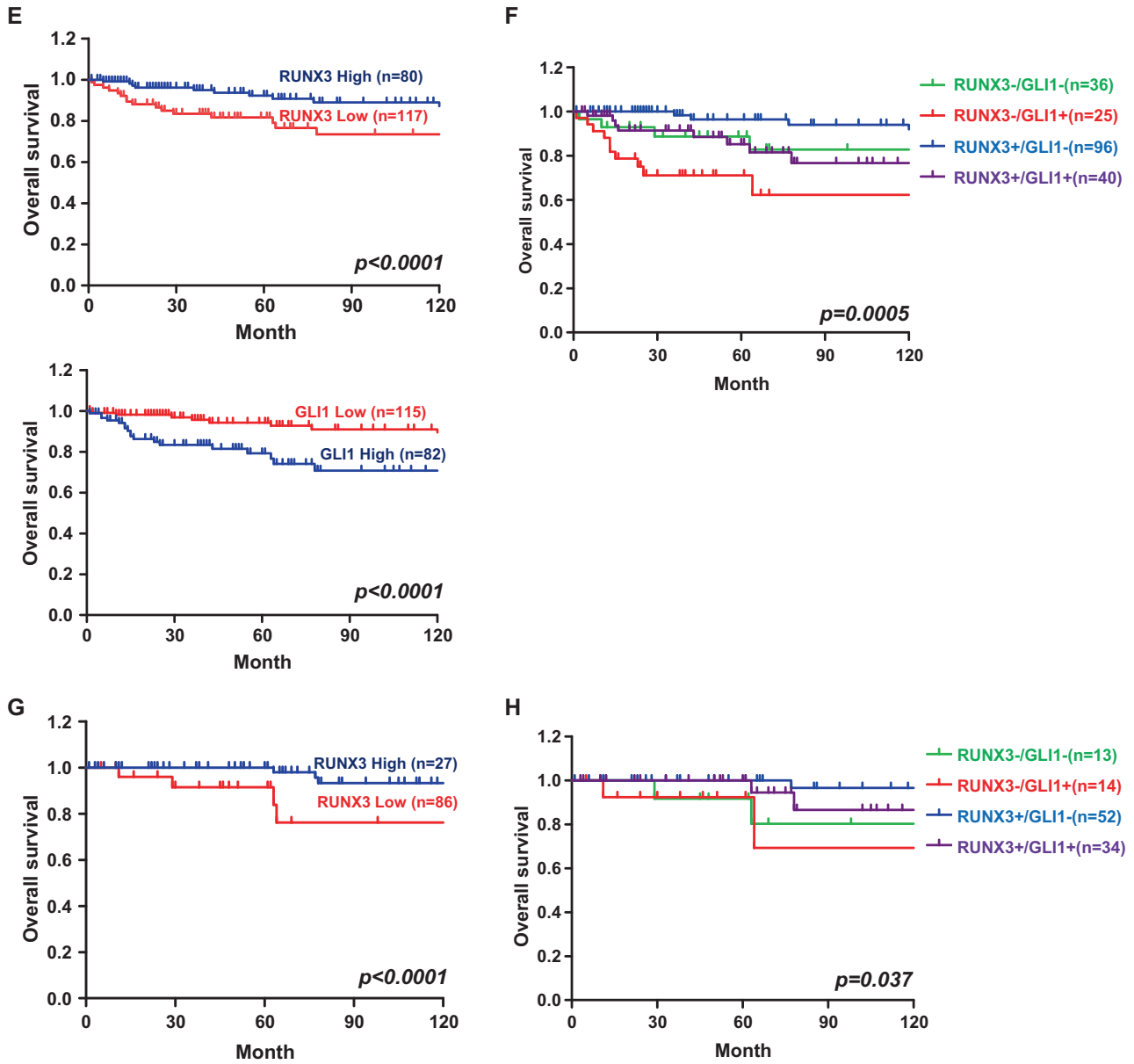

Fig. 2 (Continued)

poor survival rate than GLI1-Low patients ($p < 0.0001$) (Fig. 2e). Taken together, these results show that RUNX3-High GLI1-Low patients had the best survival rates. In contrast, RUNX3-Low GLI1-High patients had the worst survival rates ($p = 0.0005$) (Fig. 2f). These data confirm the inverse correlation between RUNX3 and GLI1 in CRC clinical specimens. To investigate the possibility as biomarker of RUNX3 to predict prognosis, we demonstrated the difference of survival by expression of RUNX3 in early stage such as stage I and II. As shown in Fig. 2g, RUNX3-High patients showed better survival rates than RUNX3-Low patients in stage I and II ($p < 0.0001$). In addition, RUNX3-High GLI1-Low patients showed the best survival rates. In contrast, RUNX3-Low GLI1-High patients showed the worst survival rates in stage I and II ($p = 0.037$) (Fig. 2h). Taken together, our data suggest that RUNX3 can be used as a biomarker in the early stages.

RUNX3 inhibits invasiveness and stemness of CRC cells

In previous reports, RUNX3 was shown to be involved in metastasis, not proliferation, apoptosis, and cell cycle [28] (Supplementary Fig. 3A, B). And thus, RUNX3 may have an important function in CRC metastasis. To explore the effect of RUNX3, we examined the protein expression of

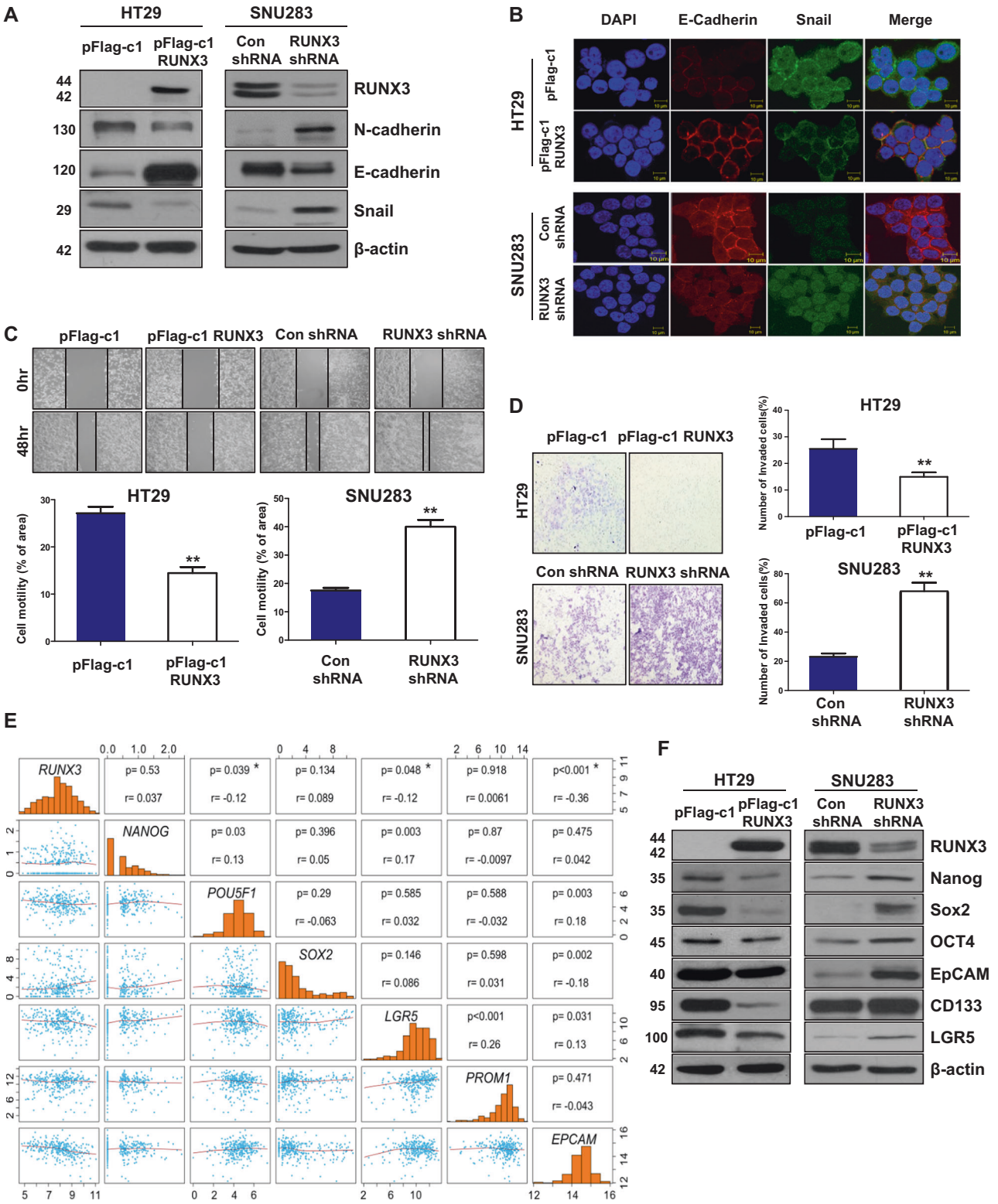

Fig. 3 (Continued)

EMT markers. In RUNX3 overexpressing cells, the epithelial marker E-cadherin was significantly increased, whereas the mesenchymal markers N-cadherin and Snail were decreased. In RUNX3 knockdown cells, E-cadherin was decreased, while N-cadherin and Snail were significantly increased (Fig. 3a). In agreement with these observations, immunofluorescence analysis confirmed that overexpression of RUNX3 inhibited EMT, while

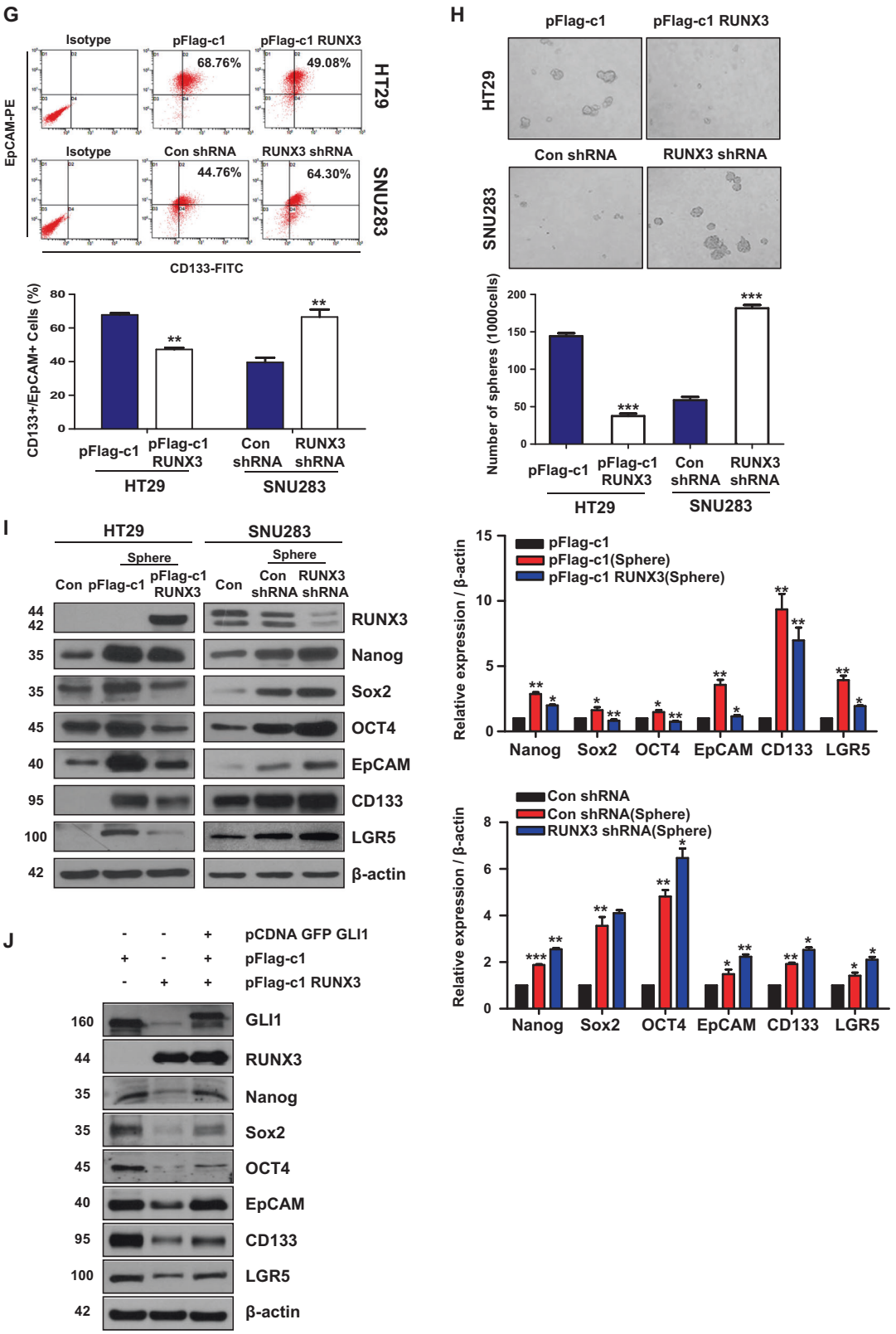

Fig. 3 (Continued)

◀ **Fig. 3** RUNX3 inhibits invasiveness and stemness of CRC cells. **a** Western blotting was performed to detect the levels of EMT markers E-cadherin, vimentin, and Snail in HT29 and SNU283 cells. β-actin was used as a loading control. **b** Immunofluorescence of E-cadherin and Snail was detected by confocal laser-scanning microscopy (original magnification, ×40). Scale bar, 10 μM. **c** Wound healing assay was performed to determine effect of cell motility in RUNX3 overexpressing cells. Cells were photographed at 0 h and incubated for 48 h. Graphs represent the average relative migration distance (bottom). **d** Transwell Matrigel invasion assay of HT29 and SNU283 cells for effect of RUNX3. Images of invasive HT29 and SNU283 cells (left). Quantitative analyses for the cell invasion through the Matrigel-coated membrane (right). **e** The Cancer Genome Atlas (TCGA) dataset was used to investigate the correlation between RUNX3 expression and cancer stemness in human. The TCGA dataset was downloaded from Xena Browser and used IlluminaHiSeq ($n = 329$) in the TCGA Colon Cancer (COAD) of the TCGA hub. Statistical analyses were conducted using R version 3.5.0 (R Foundation for Statistical Computing, Vienna, Austria). **f** Western blotting was performed to detect the levels of CSC markers (Nanog, Sox2, Oct4, EpCAM, CD133, and LGR5) in HT29 and SNU283. β-actin was used as a loading control. **g** Expression of CD133 and EpCAM in HT29 and SNU283 cells determined by flow cytometry. Cells were labeled with FITC-conjugated CD133 and PE-conjugated EpCAM antibody. Graphs represent the percentage of CD133 +/EpCAM + cells (bottom). **h** Sphere formation assay of HT29 and SNU283. Cells were cultured in serum-free DMEM/F12 with growth factor for 7 days. The graph shows the difference in the sphere numbers at 400x magnification (bottom). **i** Cells were cultured in serum-free DMEM/F12 with growth factor (EGF and FGF) for 14 days. Western blotting was performed to detect the levels of CSC markers (Nanog, Sox2, Oct4, EpCAM, CD133, and LGR5) in HT29 and SNU283. β-actin was used as a loading control. Quantitative graphs of signal intensity are shown in the right panel and were prepared using ImageJ. **j** HT29 pFlag-c1 RUNX3 cells were transfected pCDNA GFP GLI1. Western blotting was performed to detect the levels of CSC markers (Nanog, Sox2, Oct4, EpCAM, CD133, and LGR5). β-actin was used as a loading control. The data are expressed as the means of three independent experiments. ($*p < 0.05$, $**p < 0.01$, $***p < 0.001$ Student's *t*-test)

knockdown of RUNX3 enhanced EMT (Fig. 3b). We investigated the effect of RUNX3 on cell motility by a wound healing assay. Overexpression of RUNX3 significantly decreased cell motility, while knockdown of RUNX3 increased cell motility (Fig. 3c). We also examined the effect of RUNX3 on invasion of CRC cells, and found that RUNX3 overexpressing cells inhibited cell invasiveness while RUNX3 knockdown cells enhanced cell invasiveness (Fig. 3d). CSCs play critical roles in the recurrence, metastasis, and drug resistance of CRC [12]. We used the TCGA dataset to investigate the correlation of RUNX3 expression with cancer stemness and the GLI1 pathway in humans. The mRNA expression of RUNX3 was negatively correlated with CSC markers in the CRC patients of TCGA dataset. As the mRNA expression of RUNX3 increased, that of the CSC markers was decreased (Fig. 3e). This result supports our findings that RUNX3 inhibits cancer stemness. To determine whether RUNX3 regulates stemness, we measured the levels of CSC markers. Overexpression of RUNX3 resulted in the downregulation of the stem cell factors Nanog, Oct4, Sox2, EpCAM, CD133, and LGR5, whereas knockdown of RUNX3 resulted in upregulation of theses stem cell markers (Fig. 3f). These observations were also confirmed at the mRNA level. Overexpression of RUNX3 significantly decreased CSC markers, while knockdown of RUNX3 significantly increased CSC markers at the mRNA level (Supplementary Fig. 3C). In addition, we confirmed the levels of CSC markers by FACS analysis. In RUNX3 overexpressing cells, CD133 +/EpCAM + cells were decreased from 68 to 49%. In RUNX3 knockdown cells, CD133 +/EpCAM + cells were increased from 44 to 64% (Fig. 3g). Next, we constructed a stem-like CRC cell through the sphere formation culture and found that RUNX3 did not change apoptosis but cell proliferation was reduced by RUNX3 overexpression (Supplementary Fig. 4A, B). We also observed spheroid formation and found that the size and number of spheres were reduced in RUNX3 overexpressing cells. In contrast, the size and number of spheres were increased in RUNX3 knockdown cells (Fig. 3h). To examine whether RUNX3 inhibited CSC populations, we determined the effect of RUNX3 in stem-like CRC cells. At the protein level, overexpression of RUNX3 resulted in downregulation of the stem cell factors Nanog, Oct4, Sox2, EpCAM, CD133, and LGR5 in stem-like CRC cells. However, knockdown of RUNX3 resulted in upregulation of stem cell factors in stem-like CRC cells (Fig. 3i). Consistent with results at the protein level, overexpression of RUNX3 reduced the mRNA expression of the stem cell factors Nanog, Oct4, Sox2, EpCAM, CD133, and LGR5 in stem-like CRC cells. In contrast, knockdown of RUNX3 enhanced stem cell factors in stem-like CRC cells at the mRNA expression level (Supplementary Fig. 4C). To determine whether GLI1 could restore the expression of stem cell markers, we overexpressed GLI1 using pCDNA GFP GLI1 vector. Expression of stem cell markers that was decreased by overexpression of RUNX3 was restored by overexpression of GLI1 (Fig. 3j and Supplementary Fig. 4D). These results indicate that RUNX3 decreased GLI1-mediated stem cell marker. RUNX3 can repress migration, invasiveness, and cancer stemness properties of CRC cells.

RUNX3 suppresses migration, invasion, and stemness by regulating GLI1

To examine whether inhibition of metastasis and stemness by RUNX3 is GLI1-dependent, the cells were treated with 10 μM GANT61, a specific GLI inhibitor, for 48 h. As shown in Fig. 4a, the increase of GLI1 following inhibition of RUNX3 was inhibited by GANT61 or GLI1 siRNA. The increase of cell motility by RUNX3 knockdown was significantly decreased by GANT61 or GLI1 siRNA (Fig. 4b).

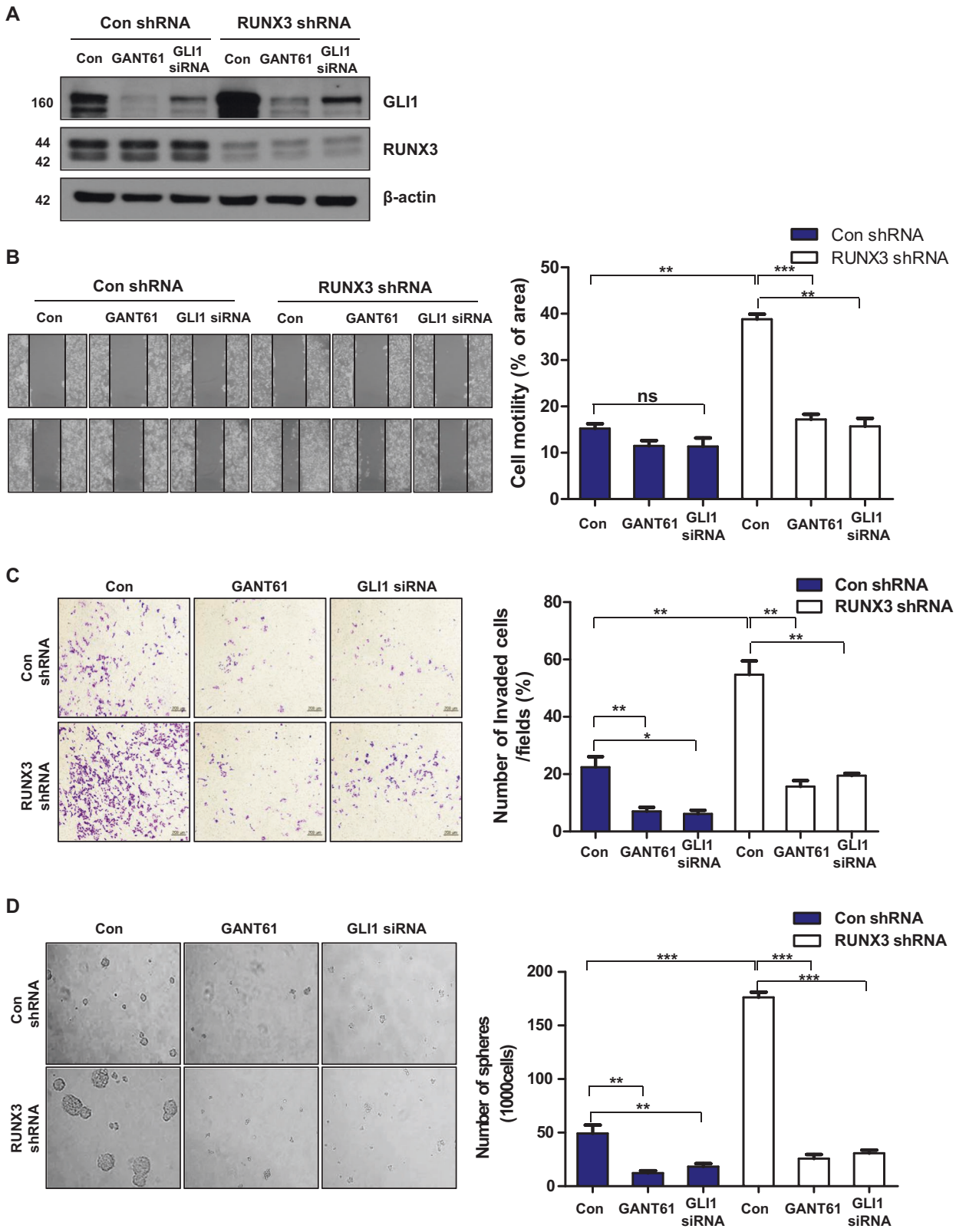

In addition, the increase of invasiveness following inhibition of RUNX3 was inhibited by treatment with GANT61 or GLI1 siRNA (Fig. 4c). These data indicate that RUNX3 suppressed cell motility and invasiveness by downregulating GLI1. Furthermore, inhibition of GLI1 prevented the increase of cell sphere size and number

◀ **Fig. 4** RUNX3 suppresses migration, invasion, and stemness by regulating GLI1. **a** SNU283 cells inhibited expression of GLI1 protein using GANT61 (10 μM; 48 h) or GLI1 siRNA, as determined by western blotting. β-actin was used as a loading control. **b** Wound healing assay was performed to determine effect of cell motility. Cells were photographed at 0 h and incubated for 48 h. **c** Transwell Matrigel invasion assay of SNU283 for effect of GANT61. Images of invasive SNU283 cells (left). Quantitative analyses for cell invasion through the Matrigel-coated membrane (right). **d** Sphere formation assay of SNU283 (Con), SNU283 (GANT61), and SNU283 (GLI1 siRNA). Cells were cultured in serum-free DMEM/F12 with growth factor for 7 days (left). The graph shows the difference in the sphere numbers at 400x magnification (right). The data are expressed as the means of three independent experiments. (*$p < 0.05$, **$p < 0.01$, ***$p < 0.001$, Student's *t*-test)

induced by RUNX3 silencing (Fig. 4d). These results suggest that RUNX3 inhibited migration, invasion, and stemness by downregulation of GLI1.

RUNX3 promotes ubiquitination of GLI1 by β-TrCP

To investigate the mechanisms by which RUNX3 regulates GLI1 expression, we confirmed the association between RUNX3 and GLI1 by immunoprecipitation (IP). The association of RUNX3 and GLI1 was enhanced in RUNX3 overexpressing cells. In contrast, the association between RUNX3 and GLI1 was weakened in RUNX3 knockdown cells (Fig. 5a). To confirm the direct interaction between RUNX3 and GLI1, we performed a GST pull-down assay. As shown in Fig. 5b, overexpression of RUNX3 increased binding to the bacterial recombinant protein GST GLI1. To map the RUNX3-GLI1 interaction domain, several deletion mutants of RUNX3 were used. The RUNX3 truncation construct (1–187) failed to co-immunoprecipitate with GLI1 (Fig. 5c), and did not alter the ubiquitination of GLI1 (Supplementary Fig 5A). These results indicate that GLI1 specifically bound to the RUNX3 truncation domain (187–234). Next, to determine whether the RUNX3-mediated decline in GLI1 occurred because of posttranslational degradation, we treated the cells with the proteasomal inhibitor MG132 and lysosome inhibitor leupeptin. As shown in Fig. 5d, the suppressive effects of RUNX3 on GLI1 protein were weakened after treatment with 2 μM MG132 for 6 h. However, the expression of GLI1 was not changed in leupeptin-treated cells, suggesting that RUNX3 inhibits GLI1 by proteasome degradation. HT29 cells were treated with or without Cyclohexamide (CHX), a protein synthesis inhibitor. The degradation rate of GLI1 was significantly increased by overexpression of RUNX3 (Supplementary Fig. 5B). Next, to identify whether RUNX3 regulated GLI1 transcription level, we confirmed the transcription level of GLI1 at short time after RUNX3 overexpression or knockdown. Overexpression or knockdown of RUNX3 not changed GLI1 mRNA level and GLI1 promoter activity (Supplementary Fig. 5D, E). These results indicate that RUNX3 does not regulate the transcription of GLI1. To determine whether RUNX3 ubiquitinates GLI1, we performed IP. As expected, overexpression of RUNX3 significantly increased the accumulation of ubiquitinated GLI1. In contrast, knockdown of RUNX3 decreased the accumulation of ubiquitinated GLI1 (Fig. 5e). These results confirm that RUNX3 can promote ubiquitination of GLI1. The studies reported that GLI1 proteasomal degradation is controlled by multiple factors. GLI1 is ubiquitinated by the E3 ligases β-TrCP, PCAF, and ITCH [24, 25]. To investigate whether the association of GLI1 with E3 ligases modulates the targeting of GLI1 for ubiquitylation, we measured the interaction between GLI1 and E3 ligases by IP. As shown in Fig. 5f, overexpression of RUNX3 enhanced the interaction between GLI1 and β-TrCP. However, the interaction between GLI1 and PCAF or ITCH was not increased. Whereas, knockdown of RUNX3 decreased the interaction between GLI1 and β-TrCP in SNU283 cells (Fig. 5g). We also examined whether GLI1 was degraded by β-TrCP-mediated protein degradation using β-TrCP siRNA. The increase of GLI1 ubiquitination resulting from overexpression of RUNX3 was decreased by β-TrCP siRNA (Fig. 5h). These data indicate that RUNX3 degraded GLI1 via β-TrCP.

RUNX3 inhibits metastasis to the lung in vivo

Finally, we performed a metastasis assay in vivo. HT29 and SNU283 cells (1×10^6) were resuspended in PBS and injected into nude mice through the lateral tail vein. As shown in Fig. 6a, HT29 pFlag-c1 RUNX3 groups showed better survival rate than HT29 pFlag-c1 groups, whereas, SNU283 Con shRNA groups showed better survival rate than SNU283 RUNX3 shRNA groups. After 9 weeks, the mice were sacrificed, and the lungs were resected for microscopic histology (Fig. 6b). The area of lungs with metastasis in mice injected with HT29 pFlag-c1 RUNX3 were significantly lower than those in mice injected with HT29 pFlag-c1 cells. whereas, the area of lung metastasis in mice injected with SNU283 RUNX3 shRNA were significantly higher than those in mice injected with SNU283 Con shRNA cells (Fig. 6c). To investigate whether inhibition of metastasis by RUNX3 was due to inhibition of GLI1, we performed an additional metastasis assay. As shown in Fig. 6e, f, lung metastasis increased by RUNX3 knockdown was decreased through inhibition of GLI1 (Fig. 6d–f). Taken together, these results suggest that RUNX3 regulates CRC metastasis via inhibition of GLI1 in vivo.

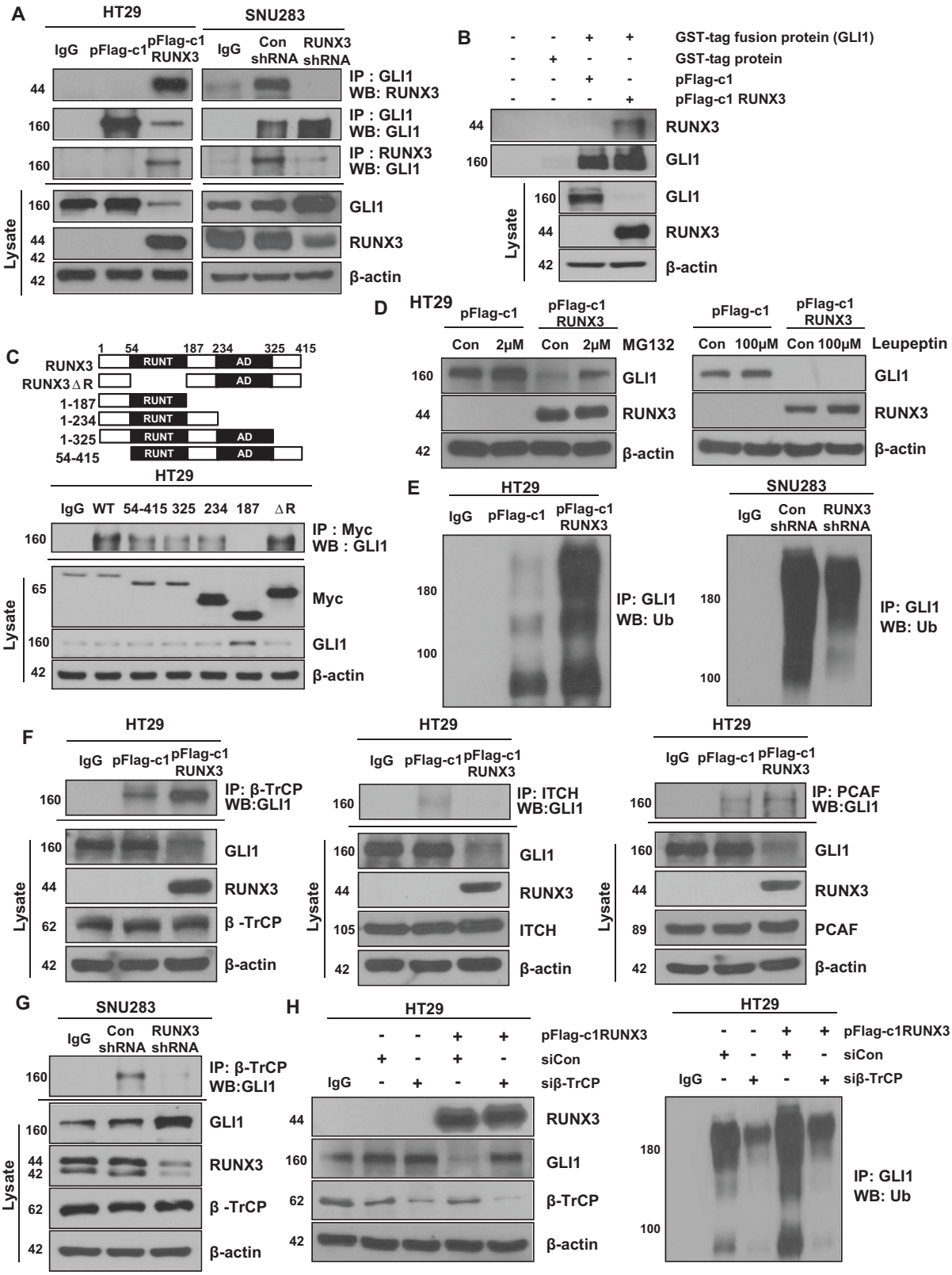
A
HT29
SNU283
IgG
pFlag-c1
pFlag-c1 RUNX3
IgG
Con shRNA
RUNX3 shRNA
IP : GLI1 WB: RUNX3
IP : GLI1 WB: GLI1
IP : RUNX3 WB: GLI1
GLI1
RUNX3
β-actin
Lysate
B
GST-tag fusion protein (GLI1)
GST-tag protein
pFlag-c1
pFlag-c1 RUNX3
RUNX3
GLI1
GLI1
RUNX3
β-actin
Lysate
C
RUNX3
RUNX3 ΔR
1-187
1-234
1-325
54-415
RUNT
AD
HT29
IgG WT 54-415 325 234 187 ΔR
IP : Myc WB : GLI1
Myc
GLI1
β-actin
Lysate
D
HT29
pFlag-c1
pFlag-c1 RUNX3
Con 2μM Con 2μM MG132
Con 100μM Con 100μM Leupeptin
GLI1
RUNX3
β-actin
E
HT29
SNU283
IgG
pFlag-c1
pFlag-c1 RUNX3
IgG
Con shRNA
RUNX3 shRNA
IP: GLI1 WB: Ub
F
HT29
IgG
pFlag-c1
pFlag-c1 RUNX3
IP: β-TrCP WB:GLI1
IP: ITCH WB:GLI1
IP: PCAF WB:GLI1
GLI1
RUNX3
β -TrCP
ITCH
PCAF
β-actin
Lysate
G
SNU283
IgG
Con shRNA
RUNX3 shRNA
IP: β-TrCP WB:GLI1
GLI1
RUNX3
β -TrCP
β-actin
Lysate
H
HT29
pFlag-c1RUNX3
siCon
siβ-TrCP
IgG
RUNX3
GLI1
β-TrCP
β-actin
IP: GLI1 WB: Ub

◀ **Fig. 5** RUNX3 promotes ubiquitination of GLI1 by β-TrCP. **a** The interaction between RUNX3 and GLI1 was tested by Co-IP. Lysates of HT29 and SNU283 cells were used for IP with GLI1 antibody and then immunoblotted with an anti-RUNX3 antibody. **b** HT29 pFlag-c1 or pFlag-c1 RUNX3 cell lysates were incubated with GST-GLI1 protein for 2 h. The lysates were immunoprecipitated with glutathione beads, followed by the eluted proteins were analyzed using western blotting. **c** Diagram showing the structure of RUNX3 truncated constructs (upper). IP using Myc antibody in HT29 cells transfected with RUNX3 truncation mutants (lower). **d** HT29 and SNU283 cells were treated with 2 μM MG132 for 6 h and 100 μM leupeptin for 24 h. Western blotting was performed. β-actin was used as a loading control. **e** Lysate of HT29 and SNU283 cells were subjected to IP with anti-GLI1 antibody and immunoblotted with anti-ubiquitin antibody. **f** The interaction between GLI1 and E3 ligases was tested by Co-IP. Lysates of HT29 cells were used for IP with anti-β-TrCP, anti-ITCH, and anti-PCAF antibody and then immunoblotted with an anti- GLI1 antibody. **g** The interaction between GLI1 and β-TrCP was tested by Co-IP. Lysates of SNU283 cells were used for IP with β-TrCP antibody and then immunoblotted with an anti- GLI1 antibody. **h** HT29 were transfected by β-TrCP siRNA. Lysate of HT29 cells was subjected to IP with anti GLI1 antibody and immunoblotted with anti-ubiquitin antibody. The data are expressed as the means of three independent experiments

Discussion

The major cause of death in CRC is metastasis and recurrence to locations such as the lymph nodes, lung, and liver [29, 30]. However, it is unknown how tumors develop the ability to metastasize to other organs. Metastasis is thought to be associated with disseminated CSCs [31]. In this study, we found that the role of RUNX3 may be based on Hh-controlled GLI1 ubiquitination, thus impacting CSCs proliferation, metastasis, and tumorigenesis.

The Hh pathway plays an important role in cancer, metastasis, angiogenesis, and stemness [32–34]. Our previous study showed that Hh signaling is highly expressed in a significant fraction of human gastric cancer patients exhibiting a significantly lower overall survival [20]. The role of the Hh pathway in tumorigenesis has been well-characterized in medulloblastoma and basal cell carcinoma (BCC). Nevertheless, the role of the Hh pathway in CRC remains controversial [35]. Indeed, some groups reported that CRC cell lines have an active Hh pathway and, in general, CRC depends on Hh signaling [36–38]. In contrast, it is known that the Hh pathway is suppressed in CRC [39–41]. Some studies showed that RUNX3 plays an oncogenic role and does not act as a tumor suppressor in skin cancers, including BCC [42]. Further, a previous study reported that RUNX3 may act as a downstream mediator of the constitutively active Hh pathway in BCC [43]. As described above, although the RUNX3 and Hh pathways have double-edged sword, our study identified a direct interaction between RUNX3 and GLI1, in which RUNX3 deficiency was associated with upregulated GLI1. We also confirmed that canonical Hh ligand-mediated activation of GLI1 was suppressed by RUNX3 (Supplementary Fig 6A). The ubiquitination levels of GLI2 and GLI3 were not changed in RUNX3 overexpressing cells (Supplementary Fig. 5C). We investigated the relationship between RUNX3 and suppressor of fused (SUFU), a major negative regulator. As shown in Supplementary Fig. 6B, overexpression of RUNX3 enhanced the interaction between SUFU and GLI1 or SUFU and RUNX3. Knockdown of SUFU decreased ubiquitination of GLI1 by RUNX3 (Supplementary Fig. 6C). RUNX3, GLI1, and SUFU formed a trimeric complex (Supplementary Fig. 6D).

An important implication of our findings is the possibility of cooperation between the SHh pathway and RUNX3 pathways in CRC, which requires further investigation. It is well known that the SHh pathway is modulated via a negative feedback loop through PTCH1, as PTCH1 itself is a positive target of GLI3 [44, 45]. The stability of GLI1 via SHh signaling is associated with a malignant phenotype in various cancers. In addition, it has been reported that increased GLI1 enhanced tumor induction in transgenic mice [46]. Unlike SHh and IHh signaling regulated GLI1 through interactions with RUNX2 and RUNX3 in a chondrogenesis mouse model [47].

Our study investigated the possibility of using RUNX3 and GLI1 as biomarkers in the patients with CRC. We demonstrated a difference of survival by expression of RUNX3 in early stages such as stages I and II. Typically, patients in these stages are not administered adjuvant chemotherapy after corrective resection of the primary tumor and show a high recurrence rate. Clinical biomarkers that detected poor prognosis patients are urgently needed.

In summary, we showed that Hh-GLI signaling, a major regulator of tumorigenesis, is suppressed by RUNX3. This phenomenon involves the ubiquitin-regulated processing of GLI1, which is mediated by functional cooperation between RUNX3 and the E3 ubiquitin ligase β-TrCP (Fig. 6g). RUNX3 also regulates the transactivation of Notch1 and, consequently, the cell proliferation fate by Notch signaling [48]. Functional crosstalk between the Notch and Hh pathways is known to occur during development and tumorigenesis, but the underlying mechanisms are unclear. Ultimately, considering the roles of Hh signaling in tumorigenesis, appropriate molecular targets should be considered for evaluation in clinical anticancer drug trials focusing on Hh signaling suppression. Our founding improves the understanding of the mechanism by which connecting to RUNX3 as a tumor suppressor and GLI1 as an oncogene occurs as it relates to the metastatic and drug resistance of CRC.

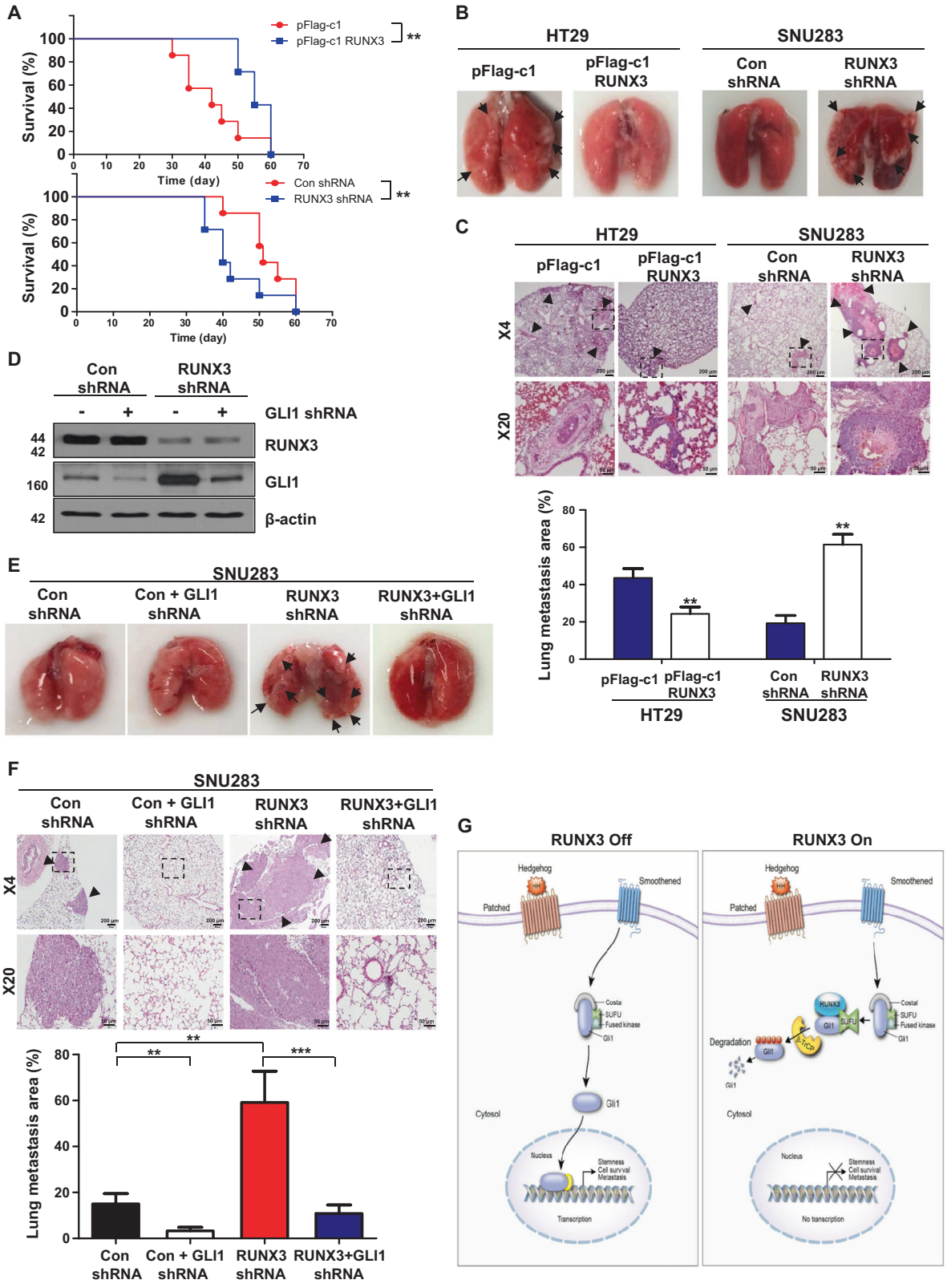
A
pFlag-c1
pFlag-c1 RUNX3
**
Survival (%)
Time (day)
Con shRNA
RUNX3 shRNA
**
B
HT29
SNU283
pFlag-c1
pFlag-c1 RUNX3
Con shRNA
RUNX3 shRNA
C
HT29
SNU283
X4
X20
Lung metastasis area (%)
D
Con shRNA
RUNX3 shRNA
GLI1 shRNA
RUNX3
GLI1
β-actin
E
SNU283
Con shRNA
Con + GLI1 shRNA
RUNX3 shRNA
RUNX3+GLI1 shRNA
F
G
RUNX3 Off
RUNX3 On
Hedgehog
Patched
Smoothened
Costa
SUFU
Fused kinase
Gli1
Cytosol
Nucleus
Transcription
Degradation
No transcription

◀ **Fig. 6** RUNX3 is important for tumorigenesis and metastasis in vivo model. **a** Percent of survival using Kaplan–Meier curves, $n = 7$ per group. **b** Representative images taken from the lungs metastasis models. **c** H&E stained lung sections from HT29 pFlag-c1 or HT29 pFlag-c1 RUNX3 and SNU283 Con shRNA or RUNX3 shRNA groups. Black arrowheads represented lung metastasis. Magnification ×4, ×20. Scale bar, 200 μm, 50 μm. **d** Western blotting was performed for detecting RUNX3 and GLI1 expression. β-actin was used as a loading control. **e** Representative images taken from the lungs metastasis models ($n = 6$). **f** H&E stained lung sections from SNU283 Con shRNA, SNU283 Con + GLI1 shRNA, SNU283 RUNX3 shRNA, and SNU283 RUNX3 + GLI1 shRNA groups. Black arrowheads represented lung metastasis. Magnification ×4, ×20. Scale bar, 200 μm, 50 μm. **g** Schematic diagram for working model of metastasis and stemness inhibition induced by RUNX3 (**$p < 0.01$, ***$p < 0.001$, Student's t-test)

Acknowledgements Vectors of pCS4-3myc-RUNX3 (full-length) and RUNX3 deletion mutant vectors fused with the Myc tag were kindly provided by Dr. SC Bae at Chungbuk National University. This research is based on data used in Bo Ram Kim's doctoral dissertation (Korea University).

Funding This work was supported by a National Research Foundation (NRF) of Korea grant funded by the Korean government (MSIP) [NRF-2017R1A6A3A11030765] and a Korea University Grant.

Author contributions BRK conceived and designed the study, provided financial support, collected and assembled the data, analyzed and interpreted the data, and wrote the paper. YJN, YAJ, SHP, and MJJ conceived and designed the study, and analyzed and interpreted the data. SHK conceived and designed the study. JLK and SYJ collected and assembled the data, and analyzed and interpreted the data. SCO and DHL conceived and designed the study, provided financial support, collected and assembled the data, analyzed and interpreted the data, wrote the paper, and provided final approval of paper. All authors discussed the results and commented on the paper.

Compliance with ethical standards

Conflict of interest The authors declare that they have no conflict of interest.

Publisher's note: Springer Nature remains neutral with regard to jurisdictional claims in published maps and institutional affiliations.

References

1. Kania MA, Bonner AS, Duffy JB, Gergen JP. The Drosophila segmentation gene runt encodes a novel nuclear regulatory protein that is also expressed in the developing nervous system. Genes Dev. 1990;4:1701–13.
2. Daga A, Karlovich CA, Dumstrei K, Banerjee U. Patterning of cells in the Drosophila eye by Lozenge, which shares homologous domains with AML1. Genes Dev. 1996;10:1194–205.
3. Ito Y. Molecular basis of tissue-specific gene expression mediated by the runt domain transcription factor PEBP2/CBF. Genes Cells. 1999;4:685–96.
4. Tracey WD, Speck NA. Potential roles for RUNX1 and its orthologs in determining hematopoietic cell fate. Semin Cell Dev Biol. 2000;11:337–42.
5. Yang S, Wei D, Wang D, Phimphilai M, Krebsbach PH, Franceschi RT. In vitro and in vivo synergistic interactions between the Runx2/Cbfa1 transcription factor and bone morphogenetic protein-2 in stimulating osteoblast differentiation. J Bone Min Res. 2003;18:705–15.
6. Bae SC, Choi JK. Tumor suppressor activity of RUNX3. Oncogene. 2004;23:4336–40.
7. Li QL, Ito K, Sakakura C, Fukamachi H, Inoue K, Chi XZ, et al. Causal relationship between the loss of RUNX3 expression and gastric cancer. Cell. 2002;109:113–24.
8. Ito K, Liu Q, Salto-Tellez M, Yano T, Tada K, Ida H, et al. RUNX3, a novel tumor suppressor, is frequently inactivated in gastric cancer by protein mislocalization. Cancer Res. 2005;65:7743–50.
9. Yanada M, Yaoi T, Shimada J, Sakakura C, Nishimura M, Ito K, et al. Frequent hemizygous deletion at 1p36 and hypermethylation downregulate RUNX3 expression in human lung cancer cell lines. Oncol Rep. 2005;14:817–22.
10. Chen F, Wang M, Bai J, Liu Q, Xi Y, Li W, et al. Role of RUNX3 in suppressing metastasis and angiogenesis of human prostate cancer. PLoS One. 2014;9:e86917.
11. He L, Zhao X, Wang H, Zhang P, Guo C, Huang C, et al. RUNX3 mediates suppression of tumor growth and metastasis of human CCRCC by regulating cyclin related proteins and TIMP-1. PLoS One. 2012;7:e32961.
12. Lobo NA, Shimono Y, Qian D, Clarke MF. The biology of cancer stem cells. Annu Rev Cell Dev Biol. 2007;23:675–99.
13. O'Brien CA, Kreso A, Jamieson CH. Cancer stem cells and self-renewal. Clin Cancer Res. 2010;16:3113–20.
14. Liu S, Dontu G, Mantle ID, Patel S, Ahn NS, Jackson KW, et al. Hedgehog signaling and Bmi-1 regulate self-renewal of normal and malignant human mammary stem cells. Cancer Res. 2006;66:6063–71.
15. Pannuti A, Foreman K, Rizzo P, Osipo C, Golde T, Osborne B, et al. Targeting Notch to target cancer stem cells. Clin Cancer Res. 2010;16:3141–52.
16. Valkenburg KC, Graveel CR, Zylstra-Diegel CR, Zhong Z, Williams BO. Wnt/beta-catenin signaling in normal and cancer stem cells. Cancers (Basel). 2011;3:2050–79.
17. Ingham PW, McMahon AP. Hedgehog signaling in animal development: paradigms and principles. Genes Dev. 2001;15:3059–87.
18. Cochrane CR, Szczepny A, Watkins DN, Cain JE. Hedgehog signaling in the maintenance of cancer stem cells. Cancers (Basel). 2015;7:1554–85.
19. Ruiz i Altaba A. Hedgehog signaling and the Gli code in stem cells, cancer, and metastases. Sci Signal. 2011;4:pt9.
20. Yoo YA, Kang MH, Lee HJ, Kim BH, Park JK, Kim HK, et al. Sonic hedgehog pathway promotes metastasis and lymphangiogenesis via activation of Akt, EMT, and MMP-9 pathway in gastric cancer. Cancer Res. 2011;71:7061–70.
21. Ruiz i Altaba A. Gli proteins and Hedgehog signaling: development and cancer. Trends Genet. 1999;15:418–25.
22. Aza-Blanc P, Lin HY, Ruiz i Altaba A, Kornberg TB. Expression of the vertebrate Gli proteins in Drosophila reveals a distribution of activator and repressor activities. Development. 2000;127:4293–301.
23. Ruiz i Altaba A, Sanchez P, Dahmane N. Gli and hedgehog in cancer: tumours, embryos and stem cells. Nat Rev Cancer. 2002;2:361–72.
24. Di Marcotullio L, Ferretti E, Greco A, De Smaele E, Po A, Sico MA, et al. Numb is a suppressor of Hedgehog signalling and targets Gli1 for Itch-dependent ubiquitination. Nat Cell Biol. 2006;8:1415–23.
25. Pandolfi S, Stecca B. Cooperative integration between HEDGEHOG-GLI signalling and other oncogenic pathways: implications for cancer therapy. Expert Rev Mol Med. 2015;17:e5.

26. Ito Y, Bae SC, Chuang LS. The RUNX family: developmental regulators in cancer. Nat Rev Cancer. 2015;15:81–95.
27. Pratap J, Wixted JJ, Gaur T, Zaidi SK, Dobson J, Gokul KD, et al. Runx2 transcriptional activation of Indian Hedgehog and a downstream bone metastatic pathway in breast cancer cells. Cancer Res. 2008;68:7795–802.
28. Kim BR, Kang MH, Kim JL, Na YJ, Park SH, Lee SI, et al. RUNX3 inhibits the metastasis and angiogenesis of colorectal cancer. Oncol Rep 2016;36:2601–8.
29. Fidler IJ. Critical factors in the biology of human cancer metastasis: twenty-eighth G.H.A. Clowes memorial award lecture. Cancer Res. 1990;50:6130–8.
30. Chaffer CL, Weinberg RA. A perspective on cancer cell metastasis. Science. 2011;331:1559–64.
31. Visvader JE, Lindeman GJ. Cancer stem cells in solid tumours: accumulating evidence and unresolved questions. Nat Rev Cancer. 2008;8:755–68.
32. Valenti G, Quinn HM, Heynen G, Lan L, Holland JD, Vogel R, et al. Cancer stem cells regulate cancer-associated fibroblasts via activation of hedgehog signaling in mammary gland tumors. Cancer Res. 2017;77:2134–47.
33. Merchant AA, Matsui W. Targeting Hedgehog—a cancer stem cell pathway. Clin Cancer Res. 2010;16:3130–40.
34. Zhao C, Chen A, Jamieson CH, Fereshteh M, Abrahamsson A, Blum J, et al. Hedgehog signalling is essential for maintenance of cancer stem cells in myeloid leukaemia. Nature. 2009;458:776–9.
35. Papadopoulos V, Tsapakidis K, Riobo Del Galdo NA, Papandreou CN, Del Galdo F, Anthoney A, et al. The prognostic significance of the hedgehog signaling pathway in colorectal cancer. Clin Colorectal Cancer. 2016;15:116–27.
36. Varnat F, Duquet A, Malerba M, Zbinden M, Mas C, Gervaz P, et al. Human colon cancer epithelial cells harbour active HEDGEHOG-GLI signalling that is essential for tumour growth, recurrence, metastasis and stem cell survival and expansion. EMBO Mol Med. 2009;1:338–51.
37. Mazumdar T, DeVecchio J, Shi T, Jones J, Agyeman A, Houghton JA. Hedgehog signaling drives cellular survival in human colon carcinoma cells. Cancer Res. 2011;71:1092–102.
38. Yoshimoto AN, Bernardazzi C, Carneiro AJ, Elia CC, Martinusso CA, Ventura GM, et al. Hedgehog pathway signaling regulates human colon carcinoma HT-29 epithelial cell line apoptosis and cytokine secretion. PLoS One. 2012;7:e45332.
39. Chatel G, Ganeff C, Boussif N, Delacroix L, Briquet A, Nolens G, et al. Hedgehog signaling pathway is inactive in colorectal cancer cell lines. Int J Cancer. 2007;121:2622–7.
40. Gerling M, Buller NV, Kirn LM, Joost S, Frings O, Englert B, et al. Stromal Hedgehog signalling is downregulated in colon cancer and its restoration restrains tumour growth. Nat Commun. 2016;7:12321.
41. van den Brink GR, Bleuming SA, Hardwick JC, Schepman BL, Offerhaus GJ, Keller JJ, et al. Indian Hedgehog is an antagonist of Wnt signaling in colonic epithelial cell differentiation. Nat Genet. 2004;36:277–82.
42. Lee JH, Pyon JK, Kim DW, Lee SH, Nam HS, Kang SG, et al. Expression of RUNX3 in skin cancers. Clin Exp Dermatol. 2011;36:769–74.
43. Salto-Tellez M, Peh BK, Ito K, Tan SH, Chong PY, Han HC, et al. RUNX3 protein is overexpressed in human basal cell carcinomas. Oncogene. 2006;25:7646–9.
44. Marigo V, Tabin CJ. Regulation of patched by sonic hedgehog in the developing neural tube. Proc Natl Acad Sci USA. 1996;93:9346–51.
45. Goodrich LV, Johnson RL, Milenkovic L, McMahon JA, Scott MP. Conservation of the hedgehog/patched signaling pathway from flies to mice: induction of a mouse patched gene by Hedgehog. Genes Dev. 1996;10:301–12.
46. Nilsson M, Unden AB, Krause D, Malmqwist U, Raza K, Zaphiropoulos PG, et al. Induction of basal cell carcinomas and trichoepitheliomas in mice overexpressing GLI-1. Proc Natl Acad Sci USA. 2000;97:3438–43.
47. Kim EJ, Cho SW, Shin JO, Lee MJ, Kim KS, Jung HS. Ihh and Runx2/Runx3 signaling interact to coordinate early chondrogenesis: a mouse model. PLoS One. 2013;8:e55296.
48. Gao J, Chen Y, Wu KC, Liu J, Zhao YQ, Pan YL, et al. RUNX3 directly interacts with intracellular domain of Notch1 and suppresses Notch signaling in hepatocellular carcinoma cells. Exp Cell Res. 2010;316:149–57.